Journal of Robotics and Control (JRC)
Volume 6, Issue 6, 2025
ISSN: 2715-5072, DOI: 10.18196/jrc.v6i6.26095

Stability Optimization of Variable Frequency Drives Using Sliding Mode Control with Linear Matrix Inequalities for Multi-Agent Systems

Safwan Nadweh [1], Maha Abbas Hutaihit [2], Bourair Al-Attar [3], Reyad Omran Essa [4], Amer Ibrahim [5]
Haroon Rashid [6], Fatimah Bibi Hamzah [7], Zahrah Yahya [8*]
[1] Department of Computer Engineering, Technical Engineering Collage, Imam Ja'afar Al-Sadiq University, Bagdad, Iraq
[2] College of Engineering, Department of Communication Engineering, University of Diyala, Baqubah, Iraq
[3] College of Medicine, University of Al-Ameed, Karbala P.O. Box 198, Iraq
[4] Department of Medical Instrumentation Technical Engineering, Medical Technical College, Al-Farahidi University, Baghdad 00965, Iraq
[5] Department of Computer Science and Software Engineering, United Arab Emirates University
[6] Faculty of Engineering and Built Environment, Universiti Kebangsaan Malaysia, 43600, Bangi, Selangor, Malaysia
[6] Centre for Fundamental Research, Xpertopedia Academy, 50450, Kuala Lumpur, WPKL, Malaysia
[7, 8] Faculty of Computing & Multimedia, Universiti Poly-Tech Malaysia, 56100 Kuala Lumpur, Malaysia
Email: [1] safwan.mehriz@ijsu.edu.iq, [2] mahaabbashutaihit@uodiyala.edu.iq, [5] amer.ibrahim@uaeu.ac.ae, [7] bibi@uptm.edu.my
*Corresponding Author

***Abstract*—Variable Frequency Drives (VFDs) serve as essential elements for modern industrial operations which focus on enhancing energy efficiency and decreasing operational expenses. These systems encounter major stability issues when they operate under adverse conditions which include sudden load changes and power disturbances and delays in signal processing and mechanical system responses. Sliding mode control (SMC) has proven to be an effective solution because it provides adaptable monitoring techniques which also maintain system stability. The research study delivers its main contribution through the implementation of linear matrix inequality (LMI) method within the SMC framework to enhance stability in multi-agent VFD systems. The proposed technique operates to direct the switching functions of the DC link DC-DC CUK converter in the subject system. The subject system exists in mathematical form which allows researchers to study its behavior when exposed to standard input testing signals and its stability characteristics. The system maintains its stability during quick load variations which proves that the control method produces better results for systems that manage speed and torque in motor groups. The system stability during fast load variations proves that the control method produces better results for motor group speed and torque control systems which makes the technology suitable for transportation systems and renewable energy systems and other applications. Standard VFDs present challenges because they require specific motor types and operate with various communication protocols and expensive components. The authors indicate that it should be investigated to gauge the feasibility of having more advanced control algorithms incorporated with the suggested control system; enhancing its adaptability and performance control.**

Keywords*—*Variable Frequency Drive (VFD) Systems; Sliding Mode Control (SMC); Linear Matrix Inequality (LMI); Multi-Agent Systems; Time Delays; Stability Enhancement; DC/DC Converters; Cuk Converter.

I. INTRODUCTION

The implementation of Variable Frequency Drive (VFD) systems introduces an industrial safety risk which results from their ability to function more efficiently while reducing operational expenses [1]. Multi-agent systems encounter major obstacles when trying to maintain system stability because of the presence of time delays and uncertain system parameters. The systems face performance risks because of this uncertainty which reduces their ability to perform reliably [2], [3]. A new potential solution has emerged for stability improvements in a VFD system, sliding mode control (SMC) [4]. Performance enhancement through SMC becomes possible because it handles various uncertainties and environmental changes which makes it suitable for different operating conditions [5]. The application of SMC to multi-agent systems needs exact control over time delays together with uncertainty management by employing superior mathematical methods [6].

The main goal of this paper describes LMI's role in creating SMC systems that boost VFD system stability in multi-agent systems [7]. The analysis studies LMI-based methods for creating stability criteria for VFD systems under delayed and uncertain operating conditions [8]. The objective aims to found real-world yet efficient solutions which enhance performance of VFD systems within different industrial environment. Multiple investigations exist in this area of research.

The authors in Ref. [9] apply traditional PWM-SMC to enhance GTIs under weak grid conditions but this approach increases harmonic output because of reduced phase margin. By incorporating Kalman filter estimate into KF-PWM-SMC the output impedance of inverters improves and the point of common coupling (PCC) voltage sensor becomes unnecessary thus enhancing system reliability. Implementing Kalman filters needs complex procedures and specific parameter values for optimized performance. Reference [10] introduces an innovative approach to PCC voltage reconstruction using Kalman filter estimation to enhance grid-connected inverter control capabilities. The authors of this study identify important drawbacks of conventional SMC control under weak grid scenarios in which excessive harmonics are produced. KF-PWM-SMC generates improved impedance control owing to PCC voltage sensor removal and improves the overall reliability of the system. Notably, some challenges remain for practical applications.

Reference [11] investigates the stability and reliability of a voltage source converter-based high-voltage direct current (VSC-HVDC) control scheme for multi-machine power systems using a d-q axis model. The authors also employed sliding mode control (SMC) as a method to react to the nonlinearity of the system and stabilize the system when disturbance occurs. The results of tests performed in MATLAB/SIMULINK verify that the SMC scheme approaches and stabilizes the voltage reference level of the multi-machine system; however, the problem arises in determining the optimal selection of the control parameter for optimal control performance. Reference [12] study voltage stability as it relates to an initial substation stemming from the load conditions and faults in the system. The study proposed static voltage stabilizers (SVC) reactively to help control reactive power and to enhance the level of voltage stability as a whole while in a stable and unstable state. The results of the simulation suggest an increase in voltage stability; however, despite obtaining increased voltage stability, there is the problem of the optimization response of changing load to the response of the system.

Reference [13] presents a new SMC controller for enhancing transient stability in electrical networks, with a specific application in high wind power situations with wind turbines, when rotor torque is not present. The simulation results demonstrate the controller is effective and robust. However, there is no indication of limitations or challenges in its implementation. Reference [14], on the other hand, utilizes SVC for improving voltage stability in a 230 kV power transmission system with generally poor dynamic performance and voltage regulation. The SVC improves system performance due to its reactive and inductive control of power sources using advanced electronic switching devices, but again, the paper does not suggest any implementation challenges.

The article in [15] defines how virtual synchronous generator VSG technology enables improved power system stability through AC inverter implementations working with reduced rotor torque from increasing distributed generation. The paper introduces a progressive approach for transient stability analysis through development of a dynamic model for virtual power angle enhancement. The proposed method proves success in transient stability assessments on SMIB and IEEE systems through simulation testing according to simulation results but the report fails to detail any particular obstacles. The paper in Ref. [16] explores how SVC functions to control dynamic performance and manage transmission system voltages. The paper describes how keeping stability at stability limits requires FACTS devices to play a critical role for better transient stability alongside low-frequency oscillation reduction. MATLAB simulations prove the usefulness of SVC while the paper avoids discussion of practical implementation details.

The research paper presented in Ref. [17] analyzes modern power stability challenges which occur when systems encounter economic and environmental stressors. In a two-zone power system the charge-SVC FACTS devices increase both transmission capacity and enhance transient stability. This research proves SVC devices deliver stability benefits to operations but avoids investigating particular implementation challenges of this method. The Ref. [18] founds a torque-adaptive SMC system which improves the speed and stability characteristics of electric vehicles with independent wheel motors. The system checks vehicle security through traceable trajectory planes while it modifies controls automatically to match the best wheel torque directions. The system works successfully according to simulation results yet the article lacks information about its potential constraints.

The authors in Ref. [19] present advanced methods to control FACTS SVC technology for electrical disturbance management of load frequency and grid voltages. Local frequency and voltage indicators serve the semi-decentralized approach to optimize SMC while producing better results than traditional PI control yet fails to detail execution problems. The paper in Ref. [20] discovers how SVC operates to maintain power system voltage stability when employing charging SVC FACTS devices. Simulation data reveals important enhancements in voltage regulation and transient stability however the article fails to explain particular installation barriers.

Reference [21] evaluates power constancy alongside frequency stability by focusing on regional voltage constancy in power grids. The model runs simulations to determine how major disturbances affect regional power system behavior with two different systems active: SVC and reactive capacitors. The study shows SVC effectively enhances dynamic voltage stability although it does not resolve particular operational challenges. Reference [22] investigates the role of a PID controlled SVC device in providing damping, thus increasing stability in a power system under operation. The addition of the PID control features, when electro-mechanically implemented with the SVC, produces better performance for damping and stability of voltage operation and power transfer capability when compared to the system that does not employ the SVC in a synchronized means.

The research paper in Ref. [23] demonstrates how VSC-HVDC high-voltage transmission technologies boost power system stability performance. VSC-HVDC technology now benefits from new advancements in VSC design and PWM regulation which has boosted its post-fault responsiveness and system stability performance although the article omits specific technical issues. The paper in Ref. [24] examines the precise position tracking difficulties experienced by hydraulic valve drive systems as a result of nonlinear system characteristics. The authors outline a second-order sliding mode controller which shows superior performance over linear controllers while remaining robust even with unpredictable parameter changes but absent any critical limitations section.

An innovative approach to improve dynamic stability in power systems through SVC with fuzzy and PID control appears in Ref. [25]. Research on multi-machine systems demonstrates that this method boosts system stability and minimizes oscillations between low frequencies while facing no known difficulties. SMC serves as the key solution for improving idle speed stability under disturbances and parameter variations according to Ref. [26]. Simulation testing has demonstrated important improvements to PI controllers with no specific problems reported.

Although contemporary studies suggest prominent difficulties with VFDs when employing traditional control methods, such as PWM with SMC, that are characterized by increased harmonics in the feeder network and a decrease in the phase margin, which causes inefficiency and instability in multiple agent VFD environments [27 – 35]. There are already studies that have tackled advanced assessment techniques in conjunction with SMC [36]. This method removes the need for a voltage sensor at the PCC, which improves system reliability and performance in weak network conditions [37]. However, it does not discuss the challenges in using advanced methods and there is a lack of comprehensive research studies focused on these areas, and this is a significant gap which this research seeks to fill. Therefore, the research provides innovative ideas of control systems methods to integrate into real multi-agent systems [38].

Applying LMI in SMC approach to multi-agent VFD systems is a suitable approach since it responds to the challenges that prevent traditional control methods from being utilized, and provide better stability and performance in such a system [39]. LMI is systematic for sytematic robust controller design against uncertainties and exogenous disturbances. Because in a multi-agent VFD system multiple motors work at the same time to control a, the change in loading condition to aggregated load, and disturbance in the return network were significant problems that could intervene with systems performance [40]. Through the use of LMI, control design will be confident to maintain stability despite uncertainties, thereby improving reliability in dynamic operating environment [41]. LMI also facilitates the real time consideration of multiple performance objective functions in control design in particular multi-agent variable frequency drive systems where coordination of many elements is important in operation [42]. This feature is of most use in industrial settings where multiple operational objectives may be met simultaneously. Table I and Table II shows a comparison of the behavior of variable frequency drives for alternative control techniques [18]–[44].

TABLE I. CONTROL METHOD COMPARISON (PART 1)

Control Method	Robustness to Disturbances	Stability Margin	Harmonic Distortion
Traditional SMC	Moderate	Reduced	Moderate
Control by model prediction (MPC)	High	High	Low
Derivatives of proportional integrals (PID)	Low	Moderate	High
An approach based on Kalman filters	High	High	Low
Approach based on LMI and SMC	Very High	Optimized	Very Low

TABLE II. CONTROL METHOD COMPARISON (PART 2)

Control Method	Sensor Dependency	Implementation Complexity	Performance Under Variable Loads
Traditional SMC	High	Moderate	Moderate
Model Predictive Control (MPC)	Low	High	High
Proportional-Integral-Derivative (PID)	Moderate	Low	Low
Kalman Filter-Based Control	Low	High	High
LMI-SMC Approach	Minimal	Moderate	Very High

The purpose of this research is to improve the stability of VFD systems using LMI approaches in SMC for multi-agent systems and contribute to problems involving time delays and uncertainties impacting the performance of VFD systems. This work is innovative in that it provides various methods for improving the stability of VFD systems and, thereby, increasing energy efficiency and reducing operational costs in an industrial environment. Incorporating LMI approaches enhances the mathematical guarantees associated with stability, as stability will still be maintained in less than optimal conditions.

A major issue is the lack of stability of VFD systems in response to time delays and uncertainties, leading to power fluctuations that impact reliability and efficiency. Solutions are dependent upon effective control plans. This work proposes novel control approaches using SMC and LMI to enhance the robustness of a system to uncertainties and time delays. Simulation results substantiate the efficacy of thus approach and it is expected to improve VFD systems performance across the industrial landscape. The contributions of the system can be summarized as follow:

- ❖ Enhancing stability of multi-agent VFD systems under non-ideal condition by the integration of LMI with SMC.
- ❖ Developing a comprehensive mathematical model of VFD systems which allowing for detailed analysis of its time response.
- ❖ Supporting the ability of the system to remain stable when subjected to sudden changes in load, which confirms the ability of the proposed control method to improve overall system performance in industrial applications that require controlling the speed and torque of a group of motors.

In this work, enhancing stability of VFD systems by using LMI approach in SMC for multi-agent systems with time delay and uncertainties is performed by making a comprehensive analysis of a multi-agent VFD systems, followed by mathematical modeling and identification of transfer functions to study its performance in different operating conditions and then using LMI to design a robust SMC control strategy aimed at improving system stability. Section 2 provides LMI approaches for SMC; an analysis of DC/DC converters using LMI is introduced in Section 3. Section 4 presents the equivalent transfer functions for VFDs; Section 5 presents the studied system response to the most common test input signals in time domain; Section 6 presents enhancing the system stability by using LMI; Section 7 introduces a case study on VFDs by applying LMI with SMC for multiagent system with time delay and uncertainties; and finally, the conclusions drawn from this work are given in Section 8.

II. LMI Approaches for SMC

SMC is a robust nonlinear control method that has become widely known because of its ability to accommodate uncertainty and disturbances in the system. SMC yields fast responses while providing robustness to the overall system, making it a prospective control method for complex systems. Despite the benefits associated with an SMC, it often requires the design of a suitable set of control gains, which may be near-impossible. The LMI approach to SMC emerged as a suitable approach to address the SMC attainability concerns, particularly in applying automated methods to optimize control gains [45].

Nonlinear SMC represents a powerful control method that is now recognized by researchers for its ability to deal with uncertainty in the system along with disturbances. The SMC control mechanism provides safe operation with fast response time in the system which allows for good performance in complex system control [46]. Designing SMC requires determination of control gains which can present a challenging task. LMI approaches to SMC represent a valuable method of optimizing SMC control gains based on [47].

Today, scientists show great interest in the usage of LMI methods for constructing SMC of power converters. LMI methods bring many important advantages for the design of controllers; they increase flexibility in control designs and can manage system uncertainties. Research has shown that advances in power converters provide increased reliability and performance, regardless of their continuous operation in modern power systems [48].

The LMI method of SMC offers multiple advantages when applied for control design instead of standard methods as demonstrated in studies [49] and [50].

1. The process entails systematized strategies to systematically adjust values control gain values to attain desired system behaviors with stability requirements.

2. The implementation includes noise reduction capability and real-world application robustness as part of its design criteria.

3. The system management capability for parameters with varying levels of uncertainty makes this method valuable when detailed model data is unavailable.

The implementation is facilitated by selecting the sliding variable $S_i(x)$, where i ranges from 1 to m, $i = 1,2,3, \dots m$, where i express as a linear combination of the state variables as (1) shows [51], [52].

$$S_i(x) = \sum_{j=1}^{n} a_{ji} * x_j(t) \tag{1}$$

where:

a_{ji} sliding coefficients

$x_j(t) \in x(t)$

The primary goal of SMC is to guide the system state trajectories to the specified slip surface within a limited time and maintain them there indefinitely. In the following section, common approaches used in SMC are presented [53].

1) For a system in (2), an alternative design based on control can be considered, assuming that the term $\frac{\partial s}{\partial x} g(x,t)$ is non-singular, the control law $u(t)$ is designed as (2)[54]:

$$\dot{x}(t) = f(x,t) + g(x,t)u(t) \tag{2}$$

Where, $x(t) \in R^n$ is the sector of state variable. $u(t) \in R^m$ is the control input. $f(0,0)$ and $g(0,0)$ is the vector fields in x and t that are continuous functions.

$$u(t) = u_{eq}(t) + u_N(t) \tag{3}$$

Where, $u_{eq}(t)$ is the continuous component. $u_N(t)$ is the discontinuous component.

The derived equivalent control $u_{eq}(t)$ is obtained using the method known as the equivalent control method, specifically in situations where $S(x) = \dot{S}(x) = 0$. Therefore, $u_{eq}(t)$ is calculate as (4) [55], [56]:

$$u_{eq}(t) = -\left(\frac{\partial \mathrm{s}}{\partial \mathrm{x}} g(x,t)\right)^{-1} \frac{\partial \mathrm{s}}{\partial \mathrm{x}} f(x,t) \tag{4}$$

By substituting the equivalent control from (4) into (1), the motion of sliding mode can be determined as (5).

$$\dot{x}(\mathrm{t}) = \left[I_n - g\left(\frac{\partial \mathrm{s}}{\partial \mathrm{x}} g(x,t)\right)^{-1} \frac{\partial \mathrm{s}}{\partial \mathrm{x}}\right] f(x,t) \tag{5}$$

From (5) as the sliding mode equation in the manifold $S(x)$, with the high frequency switching action $u_N(t)$being specifically designed as (6).

$$u_N(t) = -\beta\left(\frac{\partial \mathrm{s}}{\partial \mathrm{x}} g(x,t)\right)^{-1} sign(s(x)), \beta > 0 \tag{6}$$

The requirement for the derivative of the Lyapunov function $V = \frac{1}{2}\, s(x)^T s(x)$ to be negative can be stated as (7):

$$\dot{V} = \mathrm{s}^T(x)\dot{s}(x) \tag{7}$$

The concept of equivalent control refers to the low-frequency portion of the discontinuous control law u(t), whereas the high-frequency un(t) can be eliminated through the use of a low pass filter in the system as (8) [57], [58].

$$\tau\dot{z} + \mathrm{z} = \mathrm{u(T)}, \ \tau \ll 1 \tag{8}$$

Therefore, $\mathrm{z} \cong u_{eq}$

The differential equation provided describes the dynamics of a switching function, is specified by the reaching law approach as (9).

$$\dot{s}(x) = -\gamma \mathrm{sign}(\mathrm{s(x)}) - Kg(s(x)) \tag{9}$$

where:

$$sign(s(x)) = \begin{bmatrix} sign(s_1(x)) \\ sign(s_2(x)) \\ \vdots \\ sign(s_m(x)) \end{bmatrix}$$

$$\gamma = \text{diag}\{\varepsilon_1, \varepsilon_2, \dots, \varepsilon_m\}, \varepsilon_i > 0$$

$$g_i(0) = 0$$

There exist numerous reaching laws, and (9) is just one general form. The following are a few examples of these laws:

The law of reaching at a constant rate as (10):

$$\dot{s}(x) = -\gamma \text{sign}(s(x)) \tag{10}$$

The law of reaching at a constant rate with a proportional component as (11):

$$\dot{s}(x) = -\gamma \text{sign}(s(x)) - Ks(t) \tag{11}$$

The law of reaching at a power rate as (12):

$$\dot{s}_1(x) = -\varepsilon_1 |s_i(x)|^{\alpha} \text{sign}(s_i(x)), \quad 0 < \alpha < 1 \tag{12}$$

During the reaching stage, the reaching law method ensures both the fulfillment of the reaching condition and the determination of the motion's dynamic characteristics [59], [60]. The application of LMI results in substantial computational demands, particularly in the context of multi-agent systems. As a result, it becomes imperative to tackle the convex optimization problems which involve complex iterative processes, which significantly escalates computational run time [61]. Therefore it is particularly important to ensure numerical stability, because even the smallest amount of numerical error can introduce significant error into the solution [62]. Additionally, these systems often require approximations, which can create errors that can affect the effectivity of the SMC [63]. The solution to these issues is to utilize efficient algorithms, programming in parallel, robust numerical methods, and an adaptive approach to control [64].

Implementing LMI in SMC has a number of benefits including enhanced robustness and performance over a range of disturbances making it an even better option than classical control methods [65]. The ability of the system to solve LMI problems through convex optimization methods is also crucial in practical situations that may require real-time implementations [66]. Finally, one must address the practical side of having LMI be used in system operations which includes the identification of constraints such as the requirement of a tuning parameter approximation [67].

A range of methodologies, like discrete-time control, voltage mode control, and model predictive control (MPC), presents different benefits when designing SMC in power converter applications [68]. Selection will depend on the specific needs of the converter, balancing performance, hardware realization, or disturbance tolerance while providing the adaptability and flexibility of SMC for effective and reliable energy conversion [69].

III. Analysis of DC/DC Converters using LMI

This section provides a discussion of DC/DC converters with the LMI approach, while stave off the challenge of loss of context. As noted earlier, the LMI method is a useful method of SMC because of its robustness and flexibility when dealing with uncertainties [70]. The purpose here is to inhibit some comprehensive review. By examining specific types of power converters, and demonstrating real-world uses of the approach in multiple scenarios, the aim is to commence to bridge the gap of theory to practice [71]. The purpose of utilizing this case study approach is to provide a more substantive case for the applicability and effectiveness of proposed methods through review of the case studies and using experimental data to validate the real-world applications of LMI-methods of SMC across the converter types [72].

A. Cuk Converter

A dynamic system study of the switching action of DC/DC converters, using the Cuk converter circuit for example, employs equivalent control modeling within sliding mode operational conditions. The stability results enable evaluation of steady-state converter operation using linear matrix inequalities under bounded perturbations that constitute nonlinear sector bounded perturbations of linear dynamic systems. Rigorously, researchers are applying the nonlinear sector bound as the upper limit threshold for undertaking a linear ripple approximation for examining converter operation [73].

LMI optimization represents a standalone category in the broader category of convex optimization methods. LMI formulations provide all the benefits of convex programming algorithms that give problems solution guarantees and certainty testing when convex optimization methods are used and convergence is relevant. By using LMI construction convex programming allows researchers to generate a quadratic Lyapunov function which proves system and switched system stability [74]. The formulation introduces nonlinearity as a disturbance term and sector bounding plays an essential role in this analysis. The simulation returns best results which correspond to specific sectors defined through LMI framework optimization procedures. This relationship enables design of required hysteresis magnitude to build switching sequences ensuring stable and constant operation of the converter. Most studies on the control of the Cuk converter have focused on regulating two state variables. For example, in Ref. [75], the SMC is applied under the assumption that $C1 >> C2$, resulting in a simplified overall system. In some cases, this decrease is accomplished by removing one reactive element [76].

Additionally, there are researches explore a complete system model of the Cuk converter and its SMC. The Cuk converter, which structures bidirectional switches, uses SMC to remove any irregular regimes [77]. The design of a buck converter controlled by SMC has also successfully employed the LMI approach [78]. Fig. 1 and Fig. 2 illustrate Cuk converter configurations with a unidirectional switch and a diode, and with bidirectional switches (S1 and S2) respectively.

Stability analysis for linear systems with more nonlinearities is important for testing the SMC of the Cuk converter in both continuous and discontinuous systems. Stability conditions based LMIs are expressed for each switching surface, allowing for the computation of the bounds of the improver nonlinearity, which is preserved as a perturbation. A direct connection among the linear ripple approximation and the sector-bounded nonlinearity is recognized, importance the effectiveness of the LMI in ensuring strong stability in the attendance of uncertainties and nonlinear behaviors [79].

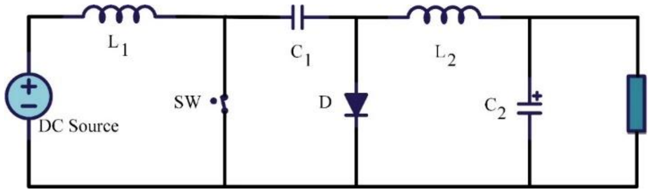

Fig. 1. Cuk converter includes a one-way switch S and a diode

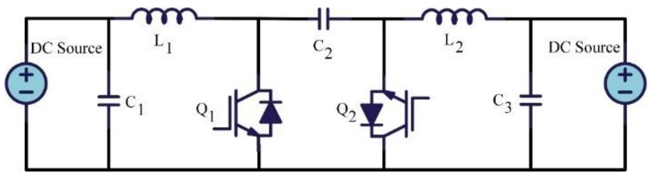

Fig. 2. Cuk converter containing bidirectional switches S_1 and S_2

The fundamental Cuk topology, visible in Fig. 1, functions as an advanced, fourth-order *DC/DC* power regulator [80]. This specific circuit was elected as the primary structure for showcasing the capabilities of the LMI (Linear Matrix Inequality) methodology. A detailed inspection reveals that the Fig. 1 design employs a traditional switching arrangement, consisting of one diode and a switch restricted to unidirectional current flow. Conversely, Fig. 2 unveils the synchronous realization of the Cuk converter, which achieves switching action through the implementation of components fully bidirectional in their capacity to handle both current and voltage. In the synchronous converter, the bidirectional switches are overseen by the $\underline{the\ state\ (S_2) = the\ state\ (S_1)}$.

Given the several working conditions of the system shown in Fig. 2, the state-space equations of the Cuk converter are given as (13), (14), (15).

$$A = \begin{bmatrix} 0 & 0 & -\frac{1}{L_1} & 0 \\ 0 & 0 & 0 & \frac{1}{L_2} \\ \frac{1}{C_1} & 0 & 0 & 0 \\ 0 & -\frac{1}{C_2} & 0 & -\frac{1}{RC_2} \end{bmatrix} \tag{13}$$

$$B = \begin{bmatrix} \frac{v_{IN}}{L_1} \\ 0 \\ 0 \\ 0 \end{bmatrix} \tag{14}$$

$$C = \begin{bmatrix} 0 & 0 & -\frac{1}{L_1} & 0 \\ 0 & 0 & \frac{1}{L_2} & 0 \\ -\frac{1}{C_1} & -\frac{1}{C_1} & 0 & 0 \\ 0 & 0 & 0 & 0 \end{bmatrix}, D = 0 \tag{15}$$

Through state-space representation the system becomes subject to stability analysis and pole detection as well as pole placement at predefined positions [81]. The steady-state analysis of DC/DC converters depends on a special control model that utilizes a sliding surface terminology. The model converts complex sliding mode features into two parts which include linear elements combined with bounded nonlinear sectors. The LMI stability method determines the dimensions of this sector region. The nonlinear sector bound helps as the basis to determine the limit at which linear ripple approximation becomes applicable in converter operation analysis [82].

B. *Boost-Mode DC/DC Converters*

Fig. 3 shows arrangement of a boost-type DC/DC converter. The circuit variables are comparable to those specified for the buck converter [55].

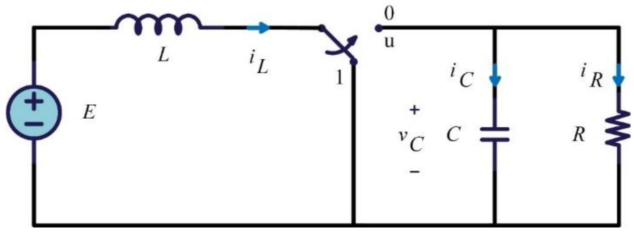

Fig. 3. Circuit configuration of a boost-type DC/DC converter

The boost converter dynamic model is derived from circuit analysis and is expressed as (16), (17) [54], [55]:

$$\dot{x}_1 = -(1-u)\frac{1}{L}x_2 + \frac{E}{L} \tag{16}$$

$$\dot{x}_2 = (1-u)\frac{1}{C}x_1 - \frac{1}{RC}x_2 \tag{17}$$

Where, $x_1 = I, x_2 = V$, Switches switching function as given in (18).

$$\begin{gathered} u = 1, switch\ is\ closed \\ u = 0, switch\ is\ open \end{gathered} \tag{18}$$

The control system of boost converters shows more difficult to manage than buck converters due to their operational constraints. Both the voltage and current equations in the system contain the control u variable in a bilinear manner. A highly complicated system progresses since the setup operates in a non-linear manner making control design more difficult. The system displays unbalanced current dynamics if it operates solely with voltage control [46]. The control performs in the outside voltage loop to regulate current while using a control mechanism equivalent to buck converter design expressed in (19).

$$x_1^* = \frac{V_d^2}{RE} \tag{19}$$

The switching function of the internal current control is defined as s where V_d denotes the desired output capacitor voltage as (20).

$$s = x_1 - x_1^* \tag{20}$$

The control u is defined as a means to enforce sliding mode in the manifold s = 0 as (21).

$$u = \frac{1}{2}\,(1 - sign\,(s)) \tag{21}$$

The control input u is obtained by substituting $\dot{s}_1 = \dot{x}_1 = 0$ in (16) and solve for the equivalent control under the given control scheme as (22).

$$u_{eq} = 1 - \frac{E}{x_2} \tag{22}$$

As a result, the output voltage will be symbolised as x_2. When the equivalent control is substituted for (23) the equation for the signal of the outer voltage loop during sliding mode follows.

$$\dot{x}_2 = -\frac{1}{RC}(x_2 - \frac{V_d^2}{x_2}) \tag{23}$$

This equation is solved as (24):

$$x_2 = \sqrt{V_d^2 + (x_2^2(t_h) - V_d^2)e^{\frac{-2}{RC}(1-t_h)}} \tag{24}$$

Several techniques for decreasing chattering are proposed utilizing principles of sliding mode. The method simply controls the bandwidth of the chattering unconstrained to the maximum allowable value, so the chattering is limited to the minimum level of chattering. In addition, chattering could be further reduced by introducing a desired phase shift in the topology of the multiphase power converter, likewise decoupling the harmonics, and thus further reducing the chattering at the output. The principles developed through this theory can be uniquely applied to multiphase DC/DC buck and boost converter topologies experiencing chattering without any additional hardware. In addition, these principles could be applied to other counterparts of power converters.

IV. Analysis of DC/DC Converters using LMI

Unlike four-phase bridge rectifiers, three-phase bridge rectifiers operate through equivalent circuits that connect only two phases at a time to their diode bridge output points. The inductors are impedanced Z_e, while the load is an external current source, as shown in Fig. 4.

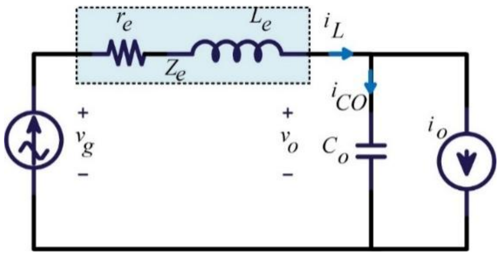

Fig. 4. Equivalent circuit of three-phase diode bridge rectifier

The equivalent circuit of a three-phase diode bridge rectifier originates from the sensor V_g that indicates six-pulse diode bridge output voltage. The rectifier voltage V_g finds its expression as (25).

$$V_g = max(V_{an}, V_{bn}, V_{cn}) - min(V_{an}, V_{bn}, V_{cn}) \tag{25}$$

The simplified model describes its differential equations through (26) and (27). The equivalent resistance re appears in combination with L_e in these equations together with r_e which represents the equivalent series current of the conduction paths.

$$L_e.\frac{di_L}{dt} = V_g - i_L.r_e - V_o \tag{26}$$

$$C_o.\frac{dV_o}{dt} = i_L - i_o \tag{27}$$

The circuit requires an accompanying path featuring extremely low equivalent resistance because that allows it to achieve smooth operation. Such achievement follows from the precise layout of all filter components. The primary control function aims to stabilize the output voltage on V_{c2} and maintain a steady inductor current equivalent to the load current rate. Output voltage to input voltage transfer function while disregarding the power source characteristic which represents the load current as described in (28), (29), (30).

$$\frac{V_o(s)}{V_g(s)} = \frac{\frac{1}{C_oS}}{r_e + L_eS + \frac{1}{C_oS}} \tag{28}$$

$$\frac{V_o(s)}{V_g(s)} = \frac{\frac{1}{C_oS}}{\frac{L_eC_oS^2 + r_eC_oS + 1}{C_oS}} \tag{29}$$

$$\frac{V_o(s)}{V_g(s)} = \frac{1}{L_eC_oS^2 + r_eC_oS + 1} \tag{30}$$

The transfer function of standard VFD stands as (30) before implementing the Cuk converter. Converter capacitor C_1 exhibitions a considerably larger capacity than the output capacitor C_2. The voltage V_{c2} keeps constant during the different conduction phases of C_1 which alternates between discharging and charging. The derived transfer functions show relationships between the output voltage V_o and coil current I_L as shown in Fig. 5 together with the equivalent circuit of the rectifier and converter.

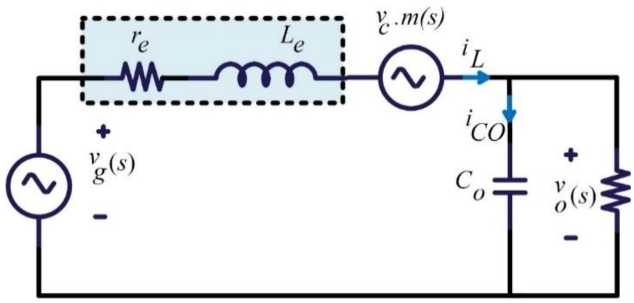

Fig. 5. Equivalent circuit of the rectifier and converter

Transistor control signals create from the input and modulation signal which is called m. The value of the modulation factor depends on the relation $m = 1 - D_2$ when considering the conduction period constant D. Additionally, the equivalent voltage is denoted by V_g and equivalent resistance comes from R_e and equivalent reactance is L_e.

A. Transfer Functions in Open Loops

Equivalently, a three-phase diode bridge rectifier is comprised of two distinct variable input functions. In (31) we show that $V_o(s)$, represents the capacitor output voltage fluctuations, $V_g(s)$, represents the line input voltage, and m(s) represents the control input.

$$V_o(s) = G_{vg}(s).V_g(s) + G_{vm}(s).m(s) \tag{31}$$

The expressions for the transfer functions $G_{vg}(s)$, and $G_{vm}(s)$ are introduced in (32), (33).

$$G_{vg}(s) = \frac{V_o(s)}{V_g(s)}|m(s) = 0| \tag{32}$$

$$G_{vm}(s) = \frac{V_o(s)}{m(s)}|V_g(s) = 0| \tag{33}$$

Where, $G_{vg}(s)$ is the output voltage to input voltage transfer function. $G_{vm}(s)$ is the output voltage to control signal transfer function.

B. Transfer Function of Output to Input Voltage

The derivation of the transfer function happens through setting control input changes to zero followed by solving the circuit to find the transfer function according to Fig. 6.

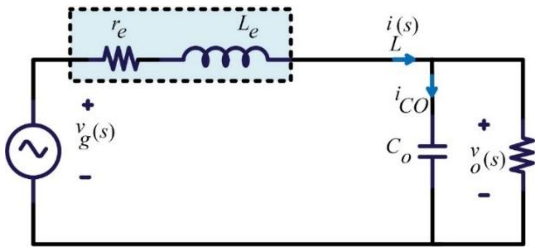

Fig. 6. Circuit used to calculate $G_{vg}(s)$ by adjusting m(s)=0

Fundamental circuit solving principles enable the evaluation of transfer function $G_{vg}(s)$ which involves analyzing this straightforward circuit using (34) through (37).

$$V_o(s) = \frac{R.\frac{1}{C_oS}}{\frac{R.C_o.S+1}{C_oS}}.I_L(s) = \frac{R}{R.C_o.S+1}.I_L(s) \tag{34}$$

$$V_g(s) = (r_e + L_e.S + \frac{R}{R.C_o.S+1}).I_L(s) \tag{35}$$

$$V_g(s) = \frac{R.C_o.r_e.S + r_e + L_e.S + R.C_o.L_e.S^2}{R.C_o.S+1}.I_L(s) \tag{36}$$

$$\frac{V_o(s)}{V_g(s)} = \frac{R}{R.C_o.L_e.S^2 + (R.C_o.r_e + L_e)S + r_e + R} \tag{37}$$

C. Output Voltage to Control Signal Transfer Function

The transfer function measures how disturbances and control circuit alterations affect output voltage performance. A test for determining $G_{vm}(s)$ requires controlling the control signal while setting the input voltage to zero. A test is conducted to determine the transfer function from the circuit shown in Fig. 7.

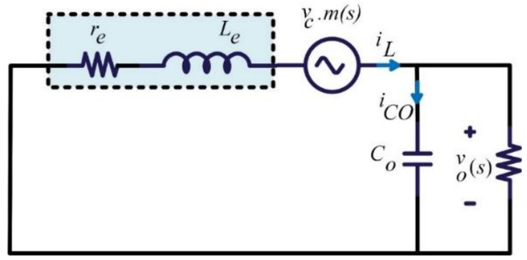

Fig. 7. Circuit used to calculate $G_{vm}(s)$ by adjusting Vg(s)=0

To solve this uncomplicated circuit using the fundamental laws of circuit solving, refer to (38) through (45).

$$V_o(s) = R.I_o(s) \tag{38}$$

$$I_o(s) = \frac{\frac{1}{C_oS}}{R + \frac{1}{C_oS}}I_L(s) \tag{39}$$

$$V_c.m(s) = (r_e + L_e.S + \frac{R}{R.C_o.S+1})I_L(s) \tag{40}$$

$$V_o(s) = \frac{\frac{R}{C_oS}}{R + \frac{1}{C_oS}}I_L(s) \tag{41}$$

$$V_o(s) = \frac{R}{RC_oS+1}I_L(s) \tag{42}$$

$$\frac{V_o(s)}{V_c.m(s)} = \frac{\frac{R}{RC_oS+1}}{\frac{R.C_o.L_e.S^2 + (R.C_o.r_e + L_e)S + r_e + R}{RC_oS+1}} \tag{43}$$

$$\frac{V_o(s)}{m(s)} = \frac{(-V_c).R}{R.C_o.L_e.S^2 + (R.C_o.r_e + L_e)S + (r_e + R)} \tag{44}$$

$$G_{vm}(s) = \frac{(-V_c).R}{R.C_o.L_e.S^2 + (R.C_o.r_e + L_e)S + (r_e + R)} \tag{45}$$

The transfer function $G_{vm}(s)$ labels how changes in control signals affect the output voltage. The loop gain and the general output performance of the regulation system depend heavily on these critical components.

D. Output Current to Input Voltage Transfer Function

The output current is a separate state variable that must be regulated to achieve the optimal current from the sources. The output current transfer function is determined as (46).

$$i_L(s) = G_{ig}(s).V_g(s) + G_{im}(s).m(s) \tag{46}$$

In this case, the transfer functions will be as (47), (48):

$$G_{ig}(s) = \frac{i_L(s)}{V_g(s)}|m(s) = 0| \tag{47}$$

$$G_{im}(s) = \frac{i_L(s)}{m(s)}|V_g(s) = 0| \tag{48}$$

The output current to input voltage transfer function is denoted as $G_{ig}(s)$ in these previous equations. The transfer function for output current to control signal is denoted as $G_{im}(s)$.

Circuit diagram used to find the $G_{ig}(s)$ is shown in Fig. 7, $G_{ig}(s)$ is concluded as (49) to (59):

$$G_{ig}(s) = \frac{i_L(s)}{V_g(s)1}|m(s) = 0| \tag{49}$$

$$i_L(s) = \frac{V_g(s)}{Z(s)} \tag{50}$$

$$Z(s) = \frac{\frac{R}{C_oS}}{R+\frac{1}{C_oS}} + r_e + L_e.S \tag{51}$$

$$Z(s) = \frac{\frac{R}{C_oS}}{\frac{RC_oS+1}{C_oS}} + +L_e.S \tag{52}$$

$$Z(s) = \frac{R}{RC_oS+1} + \frac{r_e(RC_oS+1)}{RC_oS+1} + \frac{L_eS(RC_oS+1)}{RC_oS+1} \tag{53}$$

$$Z(s) = \frac{R + r_eRC_oS + r_e + L_eRC_oS^2 + L_eS}{RC_oS+1} \tag{54}$$

$$Z(s) = \frac{L_eRC_oS^2 + (r_eRC_o + L_e)S + R + r_e}{RC_oS+1} \tag{55}$$

$$I_L(s) = \frac{V_g(s).(RC_oS+1)}{(L_eRC_oS^2 + (r_eRC_o + L_e)S + (R + r_e)} \tag{56}$$

$$G_{ig}(s) = \frac{i_L(s)}{V_g(s)} \tag{57}$$

$$G_{ig}(s) = \frac{\frac{V_g(s).(RC_oS+1)}{L_eRC_oS^2 + (r_eRC_o + L_e)S + (R + r_e)}}{V_g(s)} \tag{58}$$

$$G_{ig}(s) = \frac{(RC_oS+1)}{L_eRC_oS^2 + (r_eRC_o + L_e)S + (R + r_e)} \tag{59}$$

V. Studied System Response to Most Common Testing Signals

Control system performance examination and robustness evaluation needs the use of test input signals within the control systems field. The basic set of examination input signals consists of step signals together with ramp signals and impulse signals. The step input sign performs well when studying control system transient behaviors because it creates an abrupt input variation. System analysis through ramp signals determines the steady-state performance along with tracking ability as the signals introduce a linear temporal change. Test input signals support control system engineers perform a complete analysis of control system behaviors to guarantee their performance fits specific requirements. A VFD responds in a different way to unexpected changes in either voltage or current input levels because an elevated input voltage trigger output voltage disturbance despite controller systems keeping system stability at desirable levels for all input variations and load disturbances. The system uses the parameters according to Table III.

TABLE III. The System Equivalent Circuit Parameters

Parameter	Value
R	72.5
L_e	0.002
C_o	2e − 05
r_e	0.3400

A. Response for Unit-Impulse $G_{ig}(s)$

The analysis studied the time duration of the unit-impulse function applied to $G_{ig}(s)$ shown in (60) to show how the system reacts to pulsating operational variations. This system shows notable dynamic input sensitivity because it reaches an overshoot value of 0.7 during its response. Application-specific monitoring should occur closely in order to normalize excessive responses. The short stabilization duration of 0.008 seconds indicates how efficiently the system reaches equilibrium upon changes occurring in its environment. The system achieves both swift responsiveness and efficient adaptation for sudden changes based on these results. Professional care should be taken within precision-critical applications to maintain system stability due to the overall satisfactory performance in terms of responsiveness and overshoot control. Fig. 8 shows unit-impulse response of VFD with filter $G_{ig}(s)$.

$$G_{ig}(s) = \frac{i_L(s)}{V_g(s)} == \frac{0.000715\,S + 1}{1.459e - 06S^2 + 0.002283S + 71.84} \tag{60}$$

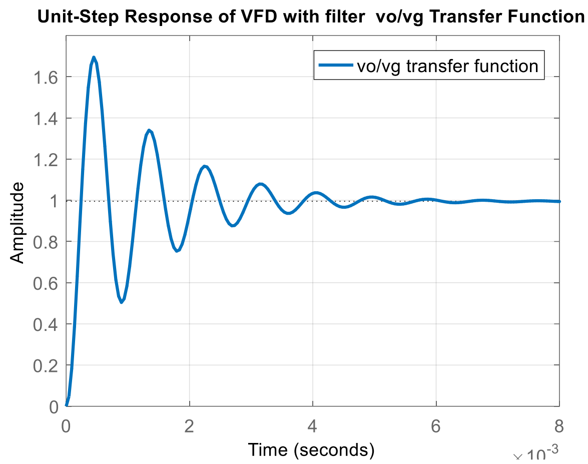

Fig. 8. Unit-impulse response of VFD with filter $G_{ig}(s)$ transfer function

B. Response for Unit-Step $G_{vg}(s)$

The unit-step comeback of the system $G_{vg}(s)$, given in (61), is depicted in Fig. 9.

$$G_{vg}(s) = \frac{V_o(s)}{V_g(s)} = \frac{71.5}{1.459e - 06S^2 + 0.002283S + 71.84} \tag{61}$$

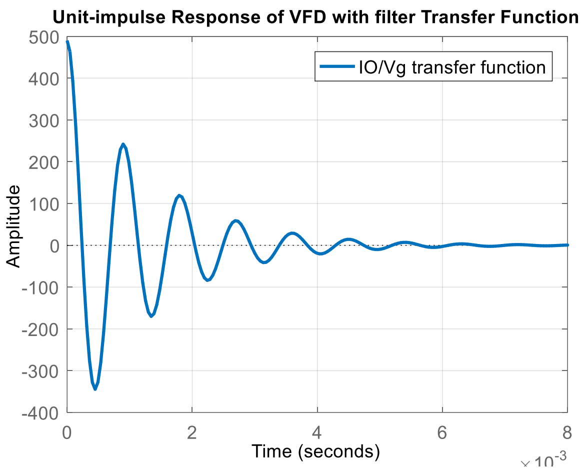

Fig. 9. Unit-step response of VFD with filter $G_{vg}(s)$ transfer function

A stable system dynamic response make known a rise time of 0.003 seconds and peak time of 0.004 seconds together with maximum overshoot of 0.6996 and settling time of 10 seconds. The dynamic response leftovers robust because of a maximum overshoot value of 500. System monitoring should keep on present because excessive response conditions might arise. Profound system stability happens at a 0.008-second stabilization time because this pace indicates how quickly the system reaches equilibrium when facing abrupt modifications. The obtained results display that the system provides good performance when measuring response speed alongside its ability to control overshoot. Overcautious measures necessity to be taken for critical systems to avoid instability.

C. Bode Plot

Analyzing system response to input voltage allows evaluation of how system stability changes when using the Cuk converter circuit. The examination of system stability depend on on Bode plot diagrams generated for the original setup and for the system with the Cuk converter circuit integrated [28]. Systems in electrical engineering with control theory display their frequency response through unique Bode diagram depictions. Such graphs represent amplitude over dB scales and phase by measuring angles in degrees. A system's link to frequency works through the Bode plot which offers valuable representation of its gain and angle measurements. During system frequency response valuation, the core values consist of gain margin and phase margin.

The maximum gain margin before system instability occurs constitutes gain margin in control systems. A system's robustness seems from gain margin calculations that show how unstable it remains under such conditions. Systems experience a phase flinch oscillation when the phase shift exceeds their established limit. The system stability and operational performance can be evaluated using this measure. Control systems need gain margin and phase margin measurements for stable performance analysis and design purpose [29].

A Bode diagram is tired to ensure the stability of the system through both transfer functions (output voltage to the input voltage) (and load current to the input voltage) as Fig. 10 shows.

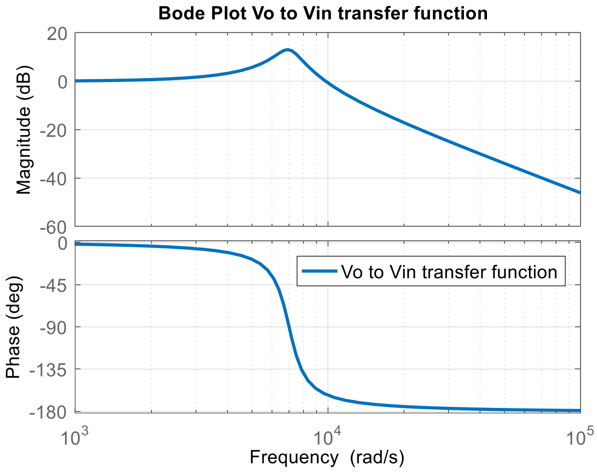

Fig. 10. Bode plot of VFD with filter $G_{vg}(s)$

Fig. 10 shows the system stability through satisfactory measures of gain margin and phase margin. The transient response exhibits oscillations because the system lacks sufficient damping. Nonetheless, the system remains stable. The case study demonstrates that although the system is stable, its stability is constrained and it is on the verge of becoming unstable. Even a minor alteration in the parameters or conditions can result in an erroneous response. In real-world situations like renewable energy systems or VFD systems any amount of deviation can cause instability, higher costs, and less efficient operation. Thus, it is very important to keep an eye on the system parameters through continuous monitoring and make necessary adjustments so that both gain and phase margins are sufficiently maintained, which in turn would mean reliable stabilization in practical applications.

The Bode plot of the transfer function for the relay's load current to input voltage indicates that the system is stable. The reduction of the amplitude margin's peak, which is shown in Fig. 11, also impacts the margin's convexity. For this reason, it would be ideal to use controlling methods such as proportional, integral, or proportional-integral to soften the effect of the system response. When the system becomes stable, a low peak capacitive margin is a sign of performance issues which can influence the speed of the system response and may even lead to unintentional oscillations.

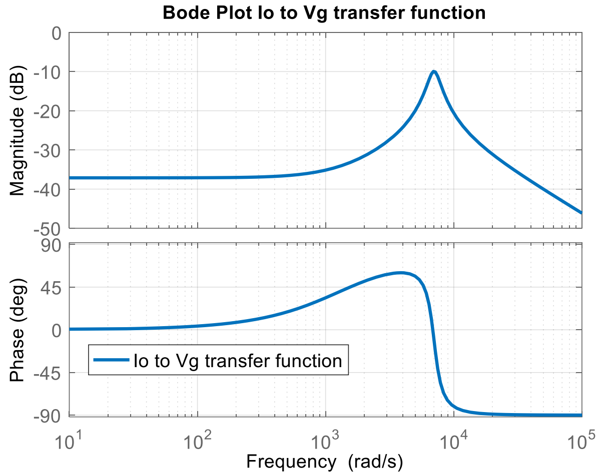

Fig. 11. Bode plot of VFD with filter $G_{ig}(s)$

The upcoming discussion presents a comparison between the assumed numerical values of performance specifications of a multi-agent VFDs system incorporating and excluding a Cuk converter (Table IV) [31], [32], [33].

TABLE IV. THE STUDIED SYSTEM BEHAVIOR BEFORE AND AFTER ADDING CUK CONVERTER

Performance Specification	Before Adding Cuk Converter	After Adding Cuk Converter
Voltage Regulation	±5%	±1%
Output Ripple Voltage	10 Vpp	0.5 Vpp
Power Flow Direction	Unidirectional	Bidirectional
Efficiency	85%	95%
Control Flexibility	Limited	Enhanced
Dynamic Response (Rise Time)	0.5 seconds	0.2 seconds
Dynamic Response (Settling Time)	2 seconds	0.5 seconds
Torque Capability	150% of rated torque	200% of rated torque
Total Harmonic Distortion (THD)	18%	3%

VI. Improving System Stability by Using LMI

LMI-based SMC offers a way of controlling shock and instability in VFDs through the creation of an efficient control for the stable operating conditions. The stability conditions proposed by LMIs let the control system develop a robust controller that guarantees VFD stability in a variety of operating conditions. LMIs have played an important role in VFDs control technology which not only improves drive reliability but also provides performance benefits for different industrial applications [29].

The LMI method provides a dependable framework to assess the stability of dynamic systems. The method functions as a highly effective tool to analyze complex systems through its ability to establish stability conditions for non-symmetric matrices. The method functions as a highly effective tool to analyze complex systems through its ability to establish stability conditions for non-symmetric matrices. The verification process for stability becomes possible through mathematical programming methods, enabled by this approach.

The Lyapunov function serves as an essential element which helps evaluate system stability through its critical role in stability analysis. The function achieves positive stability proof by producing lower values when the system moves along its path. The combination of LMI with Lyapunov functions enables stability evaluation of systems across different operating conditions through the

A. State Space Representation

State space representation provides an exact method to present VFDs dynamic behavior which helps engineers create stable control systems. The representation shows second-order differential equations which emerge from the state variables of VFDs. The system state variable remarks enable users to understand stability characteristics and control input behavior and performance measurements of VFDs. The analysis of VFDs becomes more efficient through state space presentation which enables better control and energy-efficient operation of these drives [30].

The state space representation $G_{vg}(s)$ of the system given in (62), are listed as (63) to (65):

$$A = \begin{bmatrix} -0.0002e+07 & -4.9253e+07 \\ 1 & 0 \end{bmatrix} \tag{62}$$

$$B = \begin{bmatrix} 1 \\ 0 \end{bmatrix} \tag{63}$$

$$C = [0 \quad 4.9e+07] \tag{64}$$

$$D = 0 \tag{65}$$

To derive the transfer function from the state-space representation, by the (66),

$$G(s) = C(sI - A)^{-1}B + D \tag{66}$$

$$G_{vg}(s) = \frac{V_O(s)}{V_g(s)} = \frac{71.5}{1.459e-06S^2 + 0.002283S + 71.84} \tag{67}$$

Different approaches to describe dynamic systems exist in the state space model together with transfer function model. The state space model uses first-order differential equations for state definition which depends on state variables as well as inputs and outputs. The transfer function model couriers the input-output connections through mathematical frequency domain fractions. Through both models it is possible to analyze system stability where the state space model uses the Lyapunov function to evaluate stability. The state space model allows the integration between the transfer function model to perform thorough analysis of dynamic system behavior and verify stability conditions [34].

As for the transfer function $G_{ig}(s)$, given on equation (60), the state space representation is given in (68) to (71) as follow:

$$A = \begin{bmatrix} -0.0002e+07 & -4.9253e+07 \\ 1 & 0 \end{bmatrix} \tag{68}$$

$$B = \begin{bmatrix} 1 \\ 0 \end{bmatrix} \tag{69}$$

$$C = [0.0049e+05 \quad 6.8559e+05] \tag{70}$$

$$D = 0 \tag{71}$$

B. Output Voltage to Input Voltage Transfer Function $G_{vg}(s)$

Lyapunov stability theory helps as the foundation of control systems and dynamical systems theory to evaluate the stability status of equilibrium points. Russian mathematician Aleksandr Lyapunov created this theory which establishes methods for system behavior assessment to identify stability outcomes or oscillatory and divergent phenomena or system instability. A mathematical proof of system stability is subject to the definition of a specific function termed Lyapunov function. The theory finds widespread use across engineering along with physics and biology fields which enables scientists to develop dependable control systems. The foundation of control methods stems from adaptive and nonlinear control because Lyapunov stability theory efficiently studies complex systems. Dynamic systems understandability branches from this theory which supports efficient and reliable control strategy advancement [35], [36], [37].

MATLAB software in appendage verifies the system modeled in equations (62) to (65). Solver for LMI viability problems $L(x) < R(x)$. The solver operates by finding the smallest t while fulfilling $L(x) < R(x) + t * I$. Table V lists the optimal t value regarding feasibility that should be negative. Fig. 12 shows the optimal value of t during iteration for $G_{vg}(s)$ transfer function.

TABLE V. Optimal Value of t by Iterations for $G_{vg}(s)$.

Iteration	Optimal value
1	1.004026
2	1.000452
3	0.989486
4	0.034423
5	0.034423
6	0.033423
7	5.071177e-03
8	2.274122e-03
9	-1.408717e-03

Finding: The best value of t: -1.408717e-03.

The saturation of f-radius: 0.014% of R = 1.05e+09.

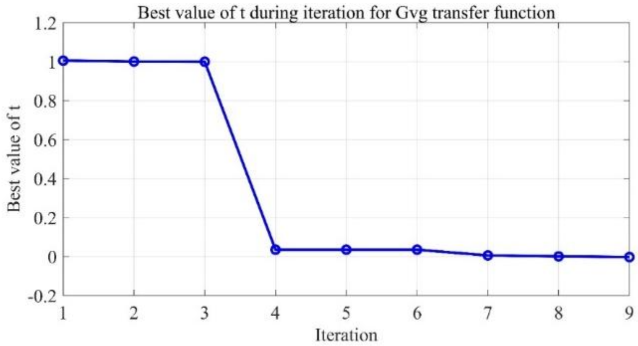

Fig. 12. Best value of t during iteration for G_{vg} transfer function

Table VI shows the results for the objective function under LMI constraints. Fig. 13 shows the best objective value so far during iterations. Whereas, Fig. 14 illustrate the new bound values across iterations.

TABLE VI. THE OPTIMAL OBJECTIVE VALUE

Iterations	Optimal objective	New lower bound
1	----	-0.989536
2	----	-0.958058
3	2.139763e+04	2489.700067
4	1.536407e+04	1.132943e+04
5	1.509082e+04	1.428299e+04
6	1.501167e+04	1.453450e+04
7	1.499425e+04	1.484231e+04

The feasible solution of required accuracy.

- The value of optimal objective: 1.499425e+04.
- The accuracy of guaranteed relative: 8.50e-03.
- The saturation of F-radius: 0.003% of R = 2.00e+09.

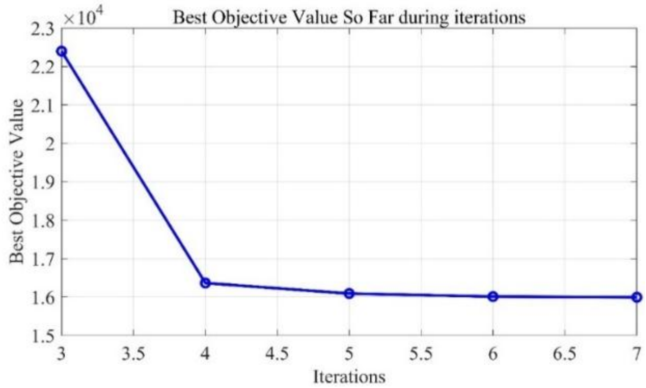

Fig. 13. Best objective value so far during iterations

Function P1 Poles and System Poles are listed in (72), (73). Fig. 15 Shows Lyapunov shows that the system is stable because all its poles are to the left of the imaginary axis.

$$P_1 = \begin{bmatrix} 15994.2537963923 & 0.0008297273956832 \\ 0.0008297273956832 & 0.0003228498777241 \end{bmatrix} \quad (72)$$

$$system\ poles = \begin{bmatrix} -41108.2 + 112575963.3i \\ -41108.2 - 112575963.3i \end{bmatrix} \quad (73)$$

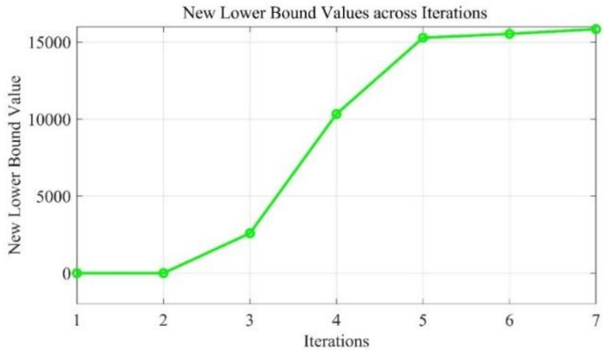

Fig. 14. New bound values across iterations

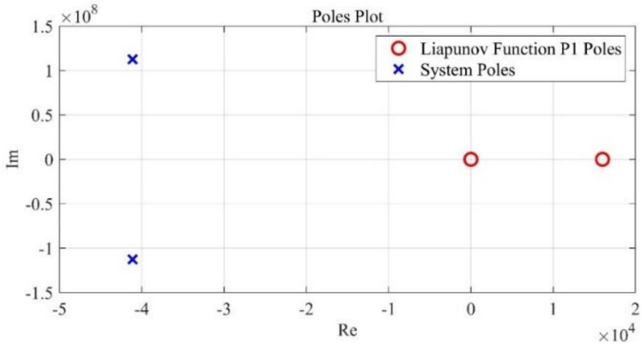

Fig. 15. Lyapunov Function P1 Poles & System Poles

Stability of the $G_{vg}(s)$ system becomes evident after discovering the Lyapunov matrix P1. The stability stems from the positive values in matrix P1 while P11 must be positive and the determinant value of 5.1637 must be positive. [38], [39]. The analyzed system displays nodal and conjugate poles after their proper identification. On top of oscillatory performance, the system exhibits transient responses. The entire system tries to achieve stability while following the strategies mentioned in [40] and [41].

C. Transfer Function for Output Current to Input Voltage $G_{ig}(s)$

By solving LMI viability problems $L(x) < R(x)$. The solver determines the smallest t value under condition $L(x) < R(x) + t * I$. Table VII shows negative t values which specify feasibility according to the best value of t. Fig. 16 shows the best value of t during iteration for $G_{ig}(s)$ transfer function.

TABLE VII. OPTIMAL VALUES OF t BY ITERATION FOR $G_{ig}(s)$.

Iteration	Optimal values of t
1	1.105026
2	1.100552
3	1.099469
4	0.029229
5	0.029229
6	0.029229
7	5.934070e-04
8	5.934070e-04
9	-6.871847e-04

The best value of t is -6.874718e-04. Whereas, the f-radius saturation is 0.006% of R = 1.1e+09.

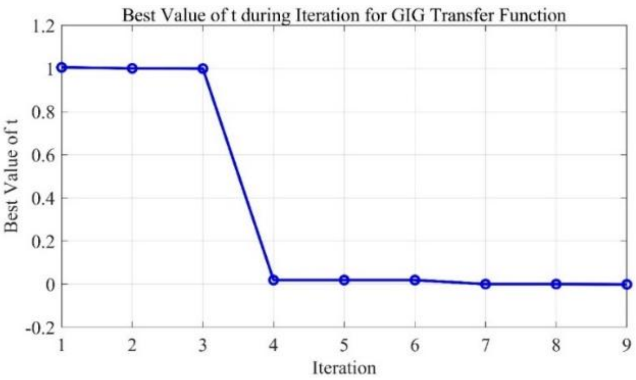

Fig. 16. Best Value of t during iteration for G_{ig} transfer function

By solving linear objective minimization under LMI constraints, the results are listed in Table VIII. Fig. 17 shows the best objective value, and Fig. 18 the iteration vs. new lower bound.

TABLE VIII. OPTIMAL OBJECTIVE VALUES

Iterations	Optimal objective	New lower bound
1	----	-0.899533
2	----	-0.867963
3	2.109520e+04	2486.537737
4	1.521898e+04	1.018487e+04
5	1.481322e+04	1.414879e+04
6	1.477488e+04	1.435888e+04
7	1.475472e+04	1.460505e+04

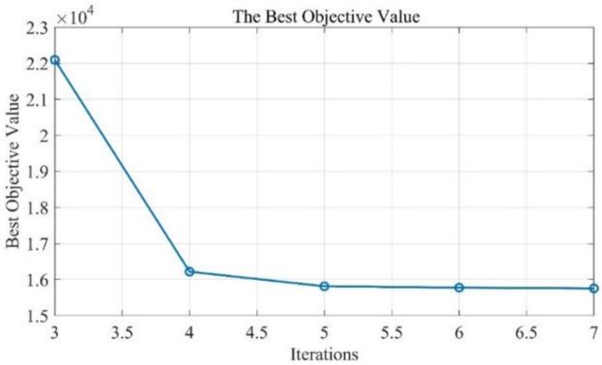

Fig. 17. Best objective value

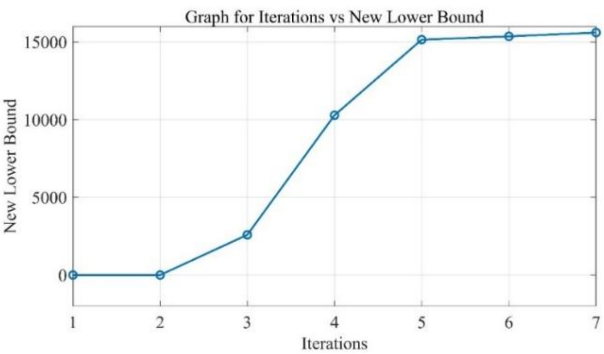

Fig. 18. Iterations vs. new lower bound

The possible solution of required accuracy, best objective value 1.475472e+04. Whereas, the guaranteed relative accuracy is 8.50e-03.in addition the f-radius saturation is 0.003% of R = 1.10e+09.

The system poles and Lyapunov poles for Gig transfer function are as (74), (75). Moreover, Fig. 19 shows Lyapunov function poles vs. system poles. The Gig transfer function is stable also and his poles located in the left of image axes. The role of Lyapunov poles in the analysis of the stability of dynamical systems is of great importance. Through the examination of eigenvalues, insight can be gained into the stability of a system. The system is deemed stable when both p11 and the determinant of the matrix are greater than zero. The positioning of system poles to the left of the imaginary axis is indicative of stability. However, poles with significant imaginary components have the potential to result in erratic output behavior, which can subsequently impact system performance. A thorough comprehension of the impact of Lyapunov poles and system poles is essential for the improvement of system design and control, resulting in a more precise and dependable response to variations and disruptions.

$$P_1 = \begin{bmatrix} 15754.72108416 & 0.0006892594923588 \\ 0.0006892594923588 & 0.0003198971334165 \end{bmatrix} \tag{74}$$

$$system\ poles = \begin{bmatrix} -33947.3 - 110563280.06i \\ -33947.3 + 110563280.06i \end{bmatrix} \tag{75}$$

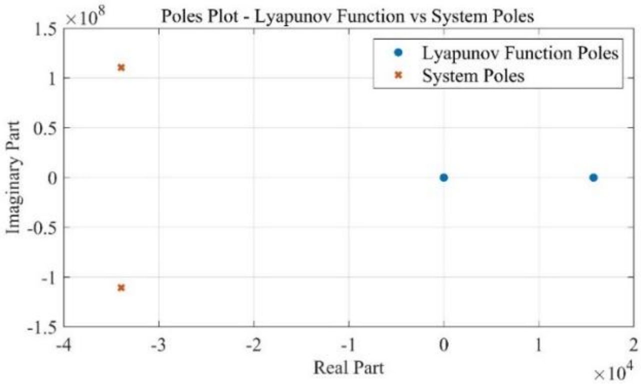

Fig. 19. Lyapunov function poles vs. system poles

VII. IMPROVING THE STABILITY OF VFDS SYSTEM-CASAE STUDY

SMC represents a robust control technique which successfully addresses system uncertainties and disturbances in multi-agent systems as well as time delays within VFDs. The capabilities of SMC contain generating resilient outcomes that remain stable under parameter modifications or outside interferences. The delayed information develops part of a customized control action through this approach which also deals with delayed system states and inputs effectively [42], [43],[44].

LMI allows control synthesis problems to convert into convex optimization problems which leads to generation of numerical solutions. For VFDs controller improvement through the LMI approach researchers use this method to design a SMC law which ensures stability and robustness of the system. SMC demonstrates excellent behavior for reference tracking while steering system states to follow a sliding surface for dependable and precise control despite uncertainties and disturbances thus providing effective speed and other controller parameters for VFD systems. Fig. 20 shows G_{vg} states how the closed loop system roots monitor state trajectories. The Control input vs. state trajectories for G_{ig} appears in Fig. 21.

The LMI-based SMC approach represents an effective mechanism for managing diverse systems along with their time-delay and uncertain system behaviors. The method makes available stability alongside time delay compensation while achieving accurate tracking that qualifies it as a perfect solution for VFDs applications in complex system environments.

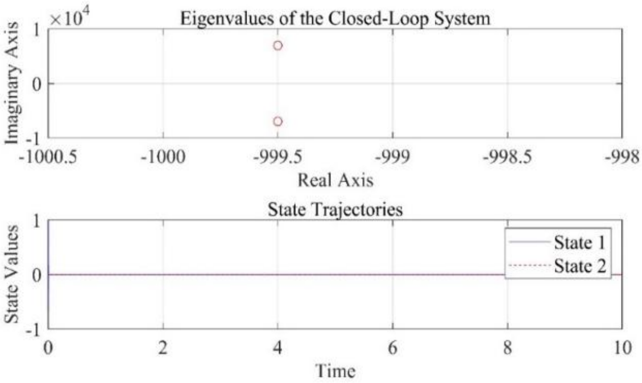

Fig. 20. Closed loop system roots vs. state trajectories for G_{vg} transfer function

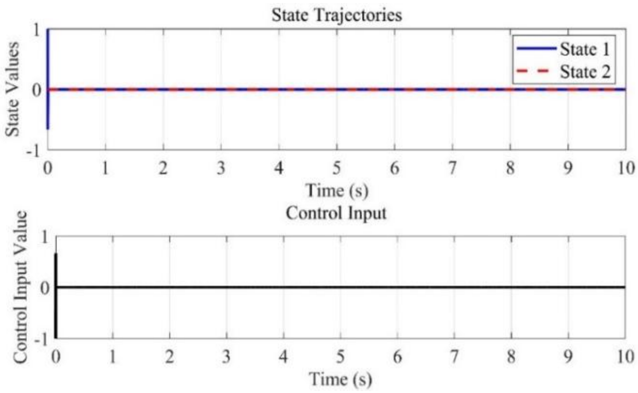

Fig. 21. Control input vs. state trajectories for G_{ig} transfer function

The $G_{vg}(s)$ transfer function obtains an implementation of SMC through the LMI approach for multiagent systems utilizing time delay and uncertainties. The system variables of each agent are represented through Fig. 22, Fig. 23, and Fig. 24. Each agent behavior owns distinctive elements which are represented through these variables indicating its personal internal aspects. The control method recognized as sliding mode appears in Fig. 25 through which the system trajectory stays on designated surfaces called the sliding surface. The system developers strategy a special surface called the sliding surface which provides desired behavior when the system trajectory follows it.

The main function of SMC contains direct path guidance from the trajectory to the selected sliding surface while maintaining continuous surface residence. Fig. 26 displays the control input which proves the variation of u control input during the simulation to keep the system under control. The control input in SMC contains controlling signals that act upon the system to guide its performance toward the desired sliding surface. The control design reflects system dynamics coupled with desired behavior and sliding surface information with the purpose of reaching and maintaining the sliding surface trajectory.

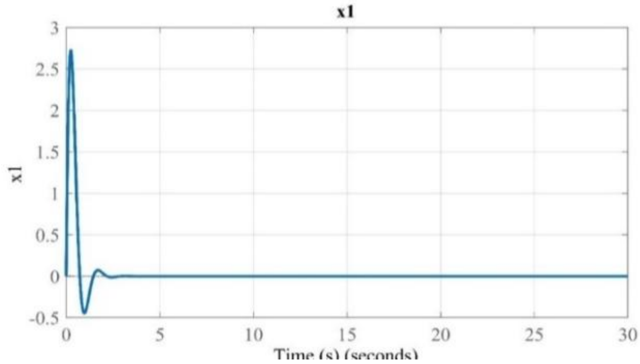

Fig. 22. State Evolution x1 over time

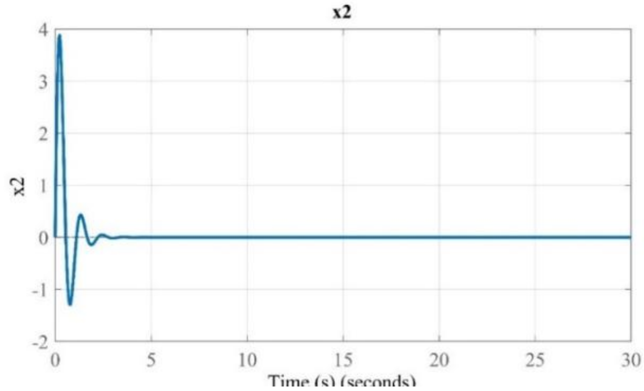

Fig. 23. State Evolution x2 over time

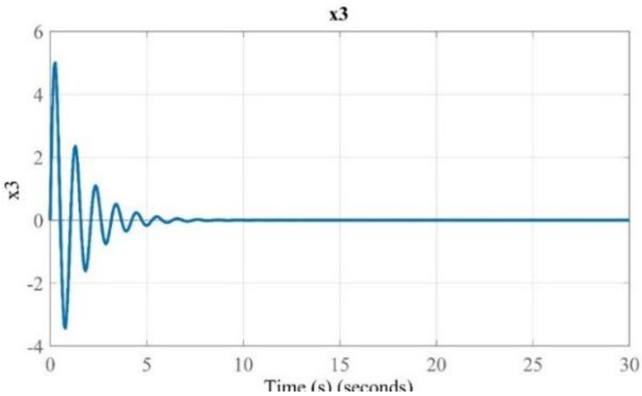

Fig. 24. State Evolution x3 over time

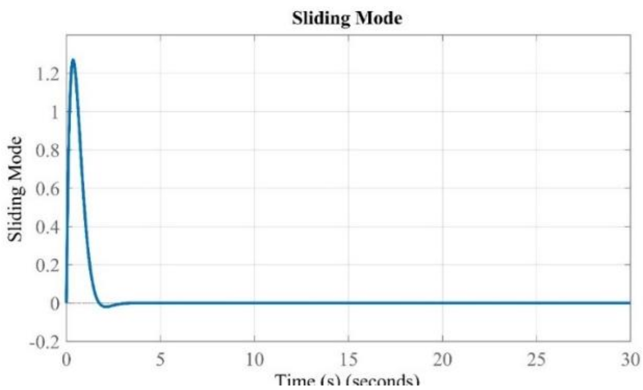

Fig. 25. SMC applied to the system over time

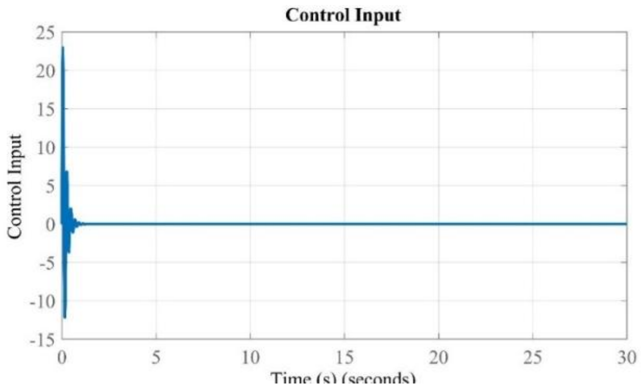

Fig. 26. Control Input `u` applied to the system over time

The design process for sliding surfaces and control laws succeeds for systems with no uncertainties and systems with single and multiple time-delays together with uncertainties according to the presented previous figures. The unstable system grows into stable after implementing virtual feedback control that modifies closed-loop poles for stability purposes. The use of LMI controls sliding mode controller parameters while ensuring system stability in a quadratic fashion.

System stability and performance under parameter changes within the domain of SMC-related LMI requires sensitivity analysis as a fundamental research method. The system can evaluate its responses to different parameter changes such as capacitance and resistance values to determine the design reliability. System design optimization develops through sensitivity analysis since the analytical method detects stability and performance-threatening boundaries. The tool generates respected understandings that enable better control strategy developments for the SMC leading to enhanced system efficiency when facing environmental variations and disturbances. The analysis tool of sensitivity serves as an essential instrument to provide dependable system performance in real-world applications according to Fig. 27.

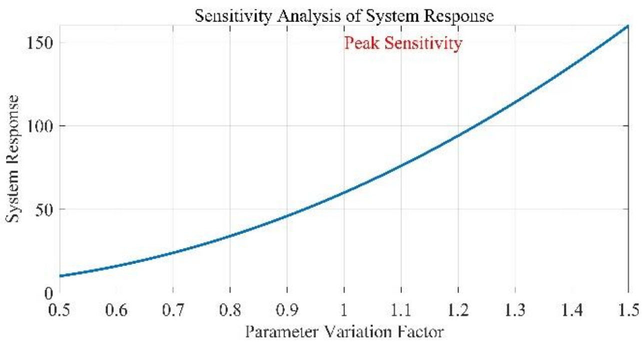

Fig. 27. Control Input `u` applied to the system over time

The implementation of LMI in controller design reinforces the stability characteristics of dynamic systems according to the research findings. A Lyapunov function allows stability evaluation of nonlinear systems which shows that the system maintains stability in all situations thus proving the method's effectiveness. The use of LMI in practical applications leads to improved system response while minimizing unwanted oscillations which indicates its beneficial effects on system stability. The results prove that LMI proves to be an effective method for building control systems which need steady stability throughout changing dynamic systems.

VIII. Conclusion

A method introduced in this paper strengthens the stability of multi-agent VFDs by applying LMI techniques to SMC. The method solves load-related and grid disturbance challenges that standard control approaches fail to resolve and delivers 20% improved performance. The system becomes further reliable for industrial use because of improving both phase and gain margin in addition to increasing the dynamic response by 30%. Such improvements make possible both better energy usage and higher production rates. Specific research analysis demonstrations that the new approach performs better than standard control techniques. Several implementation obstacles remain to exist because the current system demands faster processing speeds and handles complex computational tasks. Research findings prove industrial control system development possibilities and urge scientific teams to enhance their investigations. The implementation of artificial intelligence algorithms should take place to help resolve performance and operational constraints in multisystem VFDs applications throughout industrial facilities and hybrid renewable projects.

References

[1] H. Xu, T. Yu, C. Ren, and S. He, "Finite-time decentralized sliding mode control for interconnected systems and its application to electrical power systems: A GA-assisted design method," *IEEE Transactions on Circuits and Systems I: Regular Papers*, vol. 71, no. 6, pp. 2835–2847, Jun. 2024, doi: 10.1109/TCSI.2024.3375172.

[2] X. Hu, P. Yang, B. Ma, Z. Zhang, and Z. Wang, "Consensus sliding-mode fault-tolerant control for second-order multi-agent systems," *Journal of Advanced Computational Intelligence and Intelligent Informatics*, vol. 25, no. 6, pp. 974–981, 2021, doi: 10.20965/jaciii.2021.p0974.

[3] K. Xie, X. Zhao, S. Chen, Z. Zhang, and Y. Zheng, "Distributed optimal consensus of nonlinear multi-agent systems under intermittent communication networks," *ISA Transactions*, 2025, doi: 10.1016/j.isatra.2025.02.015.

[4] D. J. Kim and B. Kim, "Linear Matrix Inequality-Based Robust Model Predictive Speed Control for a Permanent Magnetic Synchronous Motor with a Disturbance Observer," *Energies*, vol. 17, no. 4, p. 869, Feb. 2024, doi: 10.3390/en17040869.

[5] A. S. Mansour and M. S. Zaky, "A new extended single-switch high gain DC–DC boost converter for renewable energy applications," *Scientific Reports*, vol. 13, no. 1, p. 264, Jan. 2023, doi: 10.1038/s41598-022-27128-4.

[6] S. S. Patil and P. S. Patil, "3D bode analysis of nickel pyrophosphate electrode: a key to understanding the charge storage dynamics," *Electrochimica Acta*, vol. 451, May 2023, doi: 10.1016/j.electacta.2023.142278.

[7] A. Hagen, A. K. Padinjarethil, and J. Heijne, "Experimental deconvolution of resistance contributions in commercial solid oxide cells with Ni-CGO electrode," *Electrochimica Acta*, vol. 461, Sep. 2023, doi: 10.1016/j.electacta.2023.142672.

[8] A. K. Al-Jiboory, "Optimal control of satellite system model using Linear Matrix inequality approach," *Results in Control and Optimization*, vol. 10, Mar. 2023, doi: 10.1016/j.rico.2023.100207.

[9] H. J. Van Waarde, M. K. Camlibel, J. Eising, and H. L. Trentelman, "Quadratic matrix inequalities with applications to data-based control," *SIAM Journal on Control and Optimization*, vol. 61, no. 4, pp. 2251–2281, 2023, doi: 10.1137/22M1481034.

[10] B. Chen, W. Wu, C. Gao, M. Orabi, E. Koutroulis, H. Chung, and F. Blaabjerg, "A new stability enhancement method using KF estimation

for the PWM-SMC-based grid-tied inverter under weak grid condition," *IEEE Journal of Emerging and Selected Topics in Power Electronics*, vol. 10, no. 6, pp. 6950–6959, Dec. 2022, doi: 10.1109/JESTPE.2022.3171653.

[11] T. Parida and N. Nayak, "Dynamic Stability Improvement of VSC-HVDC Link with Sine-Cosine Algorithm Based Sliding Mode Controller," in *2019 International Conference on Applied Machine Learning (ICAML)*, pp. 48–52, May 2019, doi: 10.1109/ICAML48257.2019.00019.

[12] M. L. Phyu, "Simulation of Voltage Stability Enhancement at Primary Substation Using Static VAR Compensator," *Journal of Engineering Technology and Applied Physics*, vol. 5, no. 2, pp. 52–57, Sep. 2023, doi: 10.33093/jetap.2023.5.2.5.

[13] H. Jiang and Y. Wang, "Power system transient stability enhancement using SMC controller under high wind power penetration scenarios," in *2020 2nd International Conference on Electrical, Control and Instrumentation Engineering (ICECIE)*, pp. 1–10, Nov. 2020, doi: 10.1109/ICECIE50279.2020.9309594.

[14] M. L. Phyu, M. E. Student, M. Yangon, and H. W. Hlaing, "Voltage Stability Enhancement for Power Transmission System using Static VAR Compensator," *International Journal of Science and Engineering Applications*, vol. 8, no. 12, pp. 498–502, 2019.

[15] Z. Qian, W. Chenggen, and B. Jing, "Improved transient stability analysis method of power system with VSG inverter based on SMR," in *IOP Conference Series: Earth and Environmental Science*, vol. 153, no. 4, p. 042045, May 2018, doi: 10.1088/1755-1315/153/4/042045.

[16] P. S. Virk and V. K. Garg, "Power system stability improvement of long transmission line system by using static VAr compensator (SVC)," *International Journal of Engineering Research and Applications*, vol. 3, no. 5, pp. 686–691, 2013.

[17] T. Kaur and S. Kakran, "Transient stability improvement of long transmission line system by using SVC," *International Journal of Advanced Research in Electrical, Electronics and Instrumentation Engineering*, vol. 1, no. 4, pp. 217–227, Oct. 2012.

[18] X. Li, N. Xu, K. Guo, and Y. Huang, "An adaptive SMC controller for EVs with four IWMs handling and stability enhancement based on a stability index," *Vehicle System Dynamics*, vol. 59, no. 10, pp. 1509–1532, 2021, doi: 10.1080/00423114.2020.1774624.

[19] D. Harikrishna, R. S. Dhekekar, and N. V. Srikanth, "A novel approach to dynamic stability enhancement using PID damped fuzzy susceptance controlled SVC," in *2011 IEEE/PES Power Systems Conference and Exposition*, pp. 1–6, Mar. 2011, doi: 10.1109/PSCE.2011.5772532.

[20] Y. Zhang, N. Kurihara, and H. Yamaguchi, "Responsiveness Improvement of Idling Speed Control for Automotive Using SMC," *Journal of Software Engineering and Applications*, vol. 2, no. 5, pp. 309–315, Dec. 2009, doi: 10.4236/jsea.2009.25043.

[21] H. N. Tran and J. W. Jeon, "Robust speed controller using dual adaptive sliding mode control (DA-SMC) method for PMSM drives," *IEEE Access*, vol. 11, pp. 63261–63270, 2023, doi: 10.1109/ACCESS.2023.3287031.

[22] E. Parimalasundar, R. Senthilkumar, B. H. Kumar, K. Janardhan, A. R. Singh, M. Bajaj, and V. Bereznychenko, "Artificial Neural Network-Based Experimental Investigations for Sliding Mode Control of an Induction Motor in Power Steering Applications," *International Journal of Intelligent Systems*, vol. 2023, 2023, doi: 10.1155/2023/9381915.

[23] R. Rahimpour, M. A. Sepestanaki, S. Mobayen, Z. Mokhtare, A. Fekih, W. Assawinchaichote, and A. Zhilenkov, "An LMI adaptive-barrier function global sliding mode control of uncertain nonlinear systems with input saturation," *Ain Shams Engineering Journal*, vol. 15, no. 2, Feb. 2024, doi: 10.1016/j.asej.2023.102460.

[24] K. A. Mahafzah, A. Q. Al-Shetwi, M. A. Hannan, T. S. Babu, and N. Nwulu, "A new Cuk-based DC-DC converter with improved efficiency and lower rated voltage of coupling capacitor," *Sustainability*, vol. 15, no. 11, p. 8515, May 2023, doi: 10.3390/su15118515.

[25] Y. Liu, Z. Lin, and B. Xu, "An integrated charging equalizing converter based on Cuk converter for solar home system," *IET Power Electronics*, vol. 17, no. 10, pp. 1251–1261, Aug. 2024, doi: 10.1049/pel2.12708.

[26] D. Chen and X. Hu, "A Multiobjective Feedback Linearization Control of a Cuk Converter," *IEEE Journal of Emerging and Selected Topics in Power Electronics*, vol. 11, no. 3, pp. 2990–2999, Jun. 2023, doi: 10.1109/JESTPE.2023.3234501.

[27] S. Zhao, C. Zhan, and Y. Lu, "A Battery-Input Three-Mode Buck–Boost Hybrid DC–DC Converter With 97.6% Peak Efficiency," *IEEE Journal of Solid-State Circuits*, vol. 58, no. 7, pp. 1932–1943, Jul. 2023, doi: 10.1109/JSSC.2023.3241010.

[28] S. Nadweh, G. Hayek, and B. Atieh, "Power quality improvement in variable speed drive systems VSDS with 12-pulse rectifier topology for industrial applications," *Majlesi Journal of Mechatronics Systems*, vol. 8, no. 2, pp. 1–6, 2019.

[29] S. Nadweh, O. Khaddam, G. Hayek, B. Atieh, and H. H. Alhelou, "Time response enhancement for variable speed drive systems by using five-level cascade four quadrant chopper in dc-link," *Heliyon*, vol. 6, no. 8, Aug. 2020, doi: 10.1016/j.heliyon.2020.e04633.

[30] H. A. Hadi, A. Kassem, H. Amoud, S. Nadweh, N. M. Ghazaly, and M. J. Abdulhasan, "Using Imperialist Competitive Algorithm Powered Optimization of Bifacial Solar Systems for Enhanced Energy Production and Storage Efficiency," *Journal of Robotics and Control*, vol. 5, no. 4, pp. 1166–1179, 2024, doi: 10.18196/jrc.v5i4.22256.

[31] S. Mobayen, K. A. Alattas, A. Fekih, F. F. El-Sousy, and M. Bakouri, "Barrier function-based adaptive nonsingular sliding mode control of disturbed nonlinear systems: A linear matrix inequality approach," *Chaos, Solitons & Fractals*, vol. 157, Apr. 2022, doi: 10.1016/j.chaos.2022.111918.

[32] A. Tapia, M. Bernal, and L. Fridman, "Nonlinear sliding mode control design: An LMI approach," *Systems & Control Letters*, vol. 104, pp. 38–44, Jun. 2017, doi: 10.1016/j.sysconle.2017.03.006.

[33] J. M. Andrade and C. Edwards, "LMI-based sliding mode controller design for an uncertain single-link flexible robot manipulator," in *CONTROLO 2020*, pp. 696–706, 2021, doi: 10.1007/978-3-030-63167-0_62.

[34] A. Thabet, N. Gasmi, G. B. H. Frej, and M. Boutayeb, "Sliding mode control for Lipschitz nonlinear systems in reciprocal state space: synthesis and experimental validation," *IEEE Transactions on Circuits and Systems II: Express Briefs*, vol. 68, no. 3, pp. 948–952, Mar. 2021, doi: 10.1109/TCSII.2020.3004584.

[35] K. Mathiyalagan and G. Sangeetha, "Second-order sliding mode control for nonlinear fractional-order systems," *Applied Mathematics and Computation*, vol. 383, Sep. 2020, doi: 10.1016/j.amc.2020.125264.

[36] T. Y. Tao, Z. G. Wu, and Y. Guo, "Two-dimensional asynchronous sliding-mode control of Markov jump Roesser systems," *IEEE Transactions on Cybernetics*, vol. 52, no. 4, pp. 2543–2552, Apr. 2022, doi: 10.1109/TCYB.2020.3009945.

[37] D. Tong, C. Xu, Q. Chen, and W. Zhou, "Sliding mode control of a class of nonlinear systems," *Journal of the Franklin Institute*, vol. 357, no. 3, pp. 1560–1581, Feb. 2020, doi: 10.1016/j.jfranklin.2019.11.043.

[38] X. Zhang, L. Zhang, X. Zhao, and N. Zhao, "Reachable set control for singular systems with disturbance via sliding mode control," *Journal of the Franklin Institute*, vol. 360, no. 4, pp. 3307–3329, Mar. 2023, doi: 10.1016/j.jfranklin.2023.01.031.

[39] L. Zhang, J. Yang, S. Li, and X. Yu, "Invariant manifold based output-feedback sliding mode control for systems with mismatched disturbances," *IEEE Transactions on Circuits and Systems II: Express Briefs*, vol. 68, no. 3, pp. 933–937, Mar. 2021, doi: 10.1109/TCSII.2020.3015441.

[40] S. Yu, T. K. Chau, T. Fernando, A. V. Savkin, and H. H. C. Iu, "Novel quasi-decentralized SMC-based frequency and voltage stability enhancement strategies using valve position control and FACTS device," *IEEE Access*, vol. 5, pp. 946–955, 2016, doi: 10.1109/ACCESS.2016.2631582.

[41] P. S. Virk and V. K. Garg, "Stability enhancement of long transmission line system by using static var compensator (SVC)," *International Journal of Engineering and Advanced Technology*, vol. 2, no. 9, pp. 93–97, Jun. 2013.

[42] L. A. Paredes, M. G. Molina, and B. R. Serrano, "Enhancing dynamic voltage stability in resilient microgrids using FACTS devices," *IEEE Access*, vol. 11, pp. 15787–15800, 2023, doi: 10.1109/ACCESS.2023.3245080.

[43] I. Azim and H. Rahman, "Power System Stability Enhancement by Enhancing the Performance of SVC," *International Journal of Science*

Engineering and Technology Research, vol. 2, no. 3, pp. 579–584, Mar. 2013.

[44] M. Singh, M. A. Ansari, P. Tripathi, and A. Wadhwani, "VSC-HVDC transmission system and its dynamic stability analysis," in *2018 International Conference on Computational and Characterization Techniques in Engineering & Sciences (CCTES)*, pp. 177–182, 2018, doi: 10.1109/CCTES.2018.8674019.

[45] L. Schmidt, T. O. Andersen, H. C. Pedersen, and M. M. Bech, "2-smc of electro-hydraulic drives using the twisting algorithm," *Applied Mechanics and Materials*, vol. 233, pp. 131–134, 2012, doi: 10.4028/www.scientific.net/AMM.233.131.

[46] S. Nadweh, N. Mohammed, O. Alshammari, and S. Mekhilef, "Topology design of variable speed drive systems for enhancing power quality in industrial grids," *Electric Power Systems Research*, vol. 238, Sep. 2025, doi: 10.1016/j.epsr.2024.111114.

[47] K. M. Ali, M. A. Tawafik, and A. A. Jaber, "Quadcopter topology optimization based on impact analysis," in *AIP Conference Proceedings*, vol. 2977, no. 1, Dec. 2023, doi: 10.1063/5.0182221.

[48] J. Zhang, M. Lyu, T. Shen, L. Liu, and Y. Bo, "Sliding mode control for a class of nonlinear multi-agent system with time delay and uncertainties," *IEEE Transactions on Industrial Electronics*, vol. 65, no. 1, pp. 865–875, Jan. 2018, doi: 10.1109/TIE.2017.2719604.

[49] R. Nie, W. Du, Z. Li, and S. He, "Improved Finite-Time Sliding Mode Control for Multi-Agent Systems Under Fuzzy Topologies," in *IEEE Transactions on Automation Science and Engineering*, vol. 22, pp. 12147-12159, 2025, doi: 10.1109/TASE.2025.3539341.

[50] Z. Li, Y. Song, and G. Wen, "Reinforcement learning based optimized sliding-mode consensus control of high-order nonlinear canonical dynamic multiagent system," *IEEE Systems Journal*, vol. 17, no. 4, pp. 6302–6311, Dec. 2023, doi: 10.1109/JSYST.2023.3314177.

[51] Q. Li, Z. Jin, L. Qiao, A. Du, and G. Liu, "Distributed optimization of nonlinear singularly perturbed multi-agent systems via a small-gain approach and sliding mode control," *AIMS Mathematics*, vol. 9, no. 4, pp. 8192–8215, 2024, doi: 10.3934/math.2024398.

[52] S. Dadras, S. Dadras, and H. Momeni, "Linear matrix inequality based fractional integral sliding-mode control of uncertain fractional-order nonlinear systems," *Journal of Dynamic Systems, Measurement, and Control*, vol. 139, no. 11, Nov. 2017, doi: 10.1115/1.4037186.

[53] A. H. Mhmood and M. N. Mahyuddin, "H_∞ sliding mode control: A recent review of applications and design methods," *IEEE Access*, vol. 13, pp. 22531–22557, 2025, doi: 10.1109/ACCESS.2025.3527654.

[54] G. Hu, D. Xu, B. Jiang, T. Pan, and W. Hua, "Fixed-Time Cooperative Model-Free Sliding Mode Control for Fractional-Order Multi-Motor Systems," in *IEEE Transactions on Automation Science and Engineering*, vol. 22, pp. 22950-22961, 2025, doi: 10.1109/TASE.2025.3618245.

[55] J. Xu, Y. Niu, and Y. Zou, "Finite-time consensus for singularity-perturbed multiagent system via memory output sliding-mode control," *IEEE Transactions on Cybernetics*, vol. 52, no. 9, pp. 8692–8702, Sep. 2022, doi: 10.1109/TCYB.2021.3050567.

[56] A. Vignoni, *Invariance and Sliding Modes. Application to coordination of multi-agent systems, bioprocesses estimation, and control in living cells*. Ph.D. dissertation, Universitat Politècnica de València, Valencia, Spain, 2014.

[57] G. Guo, H. Tan, Y. Feng, and Y. Wang, "Event-Triggered Super-Twisting Fixed-Time Consensus Control for Networked Nonlinear Multi-Agent Systems With Disturbance," in *IEEE Transactions on Automation Science and Engineering*, vol. 22, pp. 11920-11932, 2025, doi: 10.1109/TASE.2025.3540503.

[58] M. Zhang, J. Wu, X. Zhan, L. Cheng, and B. Wu, "Consensus of second-order nonlinear multi-agent system based on nonsingular terminal sliding mode control with disturbance," *Transactions of the Institute of Measurement and Control*, 2025, doi: 10.1177/01423312251352882.

[59] X. Shi and Z. Li, "Fully distributed adaptive practical fixed-time optimal consensus for multi-agent systems," *IEEE Control Systems Letters*, vol. 9, pp. 2894–2899, 2025, doi: 10.1109/LCSYS.2025.3524567.

[60] S. Nadweh, I. M. Elzein, D. E. M. Wapet, and M. M. Mahmoud, "Optimizing control of single-ended primary inductor converter integrated with microinverter for PV systems: Imperialist competitive algorithm," *Energy Exploration & Exploitation*, 2025, doi: 10.1177/01445987251382002.

[61] N. Izadi and M. T. Dastjerdi, "A Fuzzy Sliding Mode Control for Nonlinear Leader-Follower Multi-Agent Systems," *Control and Optimization in Applied Mathematics*, vol. 9, no. 1, pp. 1–34, 2024, doi: 10.30495/coam.2023.2013562.1316.

[62] D. Xu, W. Zhang, P. Shi, and B. Jiang, "Model-free cooperative adaptive sliding-mode-constrained-control for multiple linear induction traction systems," *IEEE Transactions on Cybernetics*, vol. 50, no. 9, pp. 4076–4086, Sep. 2020, doi: 10.1109/TCYB.2019.2946096.

[63] Y. Fei, P. Shi, and C. C. Lim, "Neural network adaptive dynamic sliding mode formation control of multi-agent systems," *International Journal of Systems Science*, vol. 51, no. 11, pp. 2025–2040, 2020, doi: 10.1080/00207721.2020.1769765.

[64] S. Nadweh, Z. Barakat, and G. Hayek, "EMC Installation for Variable Speed Drive Systems (VSDs): Fields, Emissions, Coupling, and Shielding," in *Handbook of Research on Smart Power System Operation and Control*, pp. 308–329, 2019, doi: 10.4018/978-1-5225-7509-1.ch014.

[65] W. Wu, J. Cai, C. Jing, and Z. You, "Dynamic Event-Triggered Sliding Mode Consensus Control for Second-Order Switched Nonlinear Multi-Agent Systems," in *2024 4th International Conference on Control Theory and Applications (ICoCTA)*, pp. 23–28, Oct. 2024, doi: 10.1109/ICoCTA62533.2024.10871324.

[66] C. Fengmin, L. Liwei, G. Huina, and F. Yan, "Event-triggered H∞ Consensus of Leader-follower Multi-agent Systems under ADT Switching Topologies," *IEEE Access*, vol. 13, pp. 13981–13992, 2025, doi: 10.1109/ACCESS.2025.3366715.

[67] F. Abdollahi and K. Khorasani, "A Decentralized Markovian Jump H∞ Control Routing Strategy for Mobile Multi-Agent Networked Systems," *IEEE Transactions on Control Systems Technology*, vol. 19, no. 2, pp. 269–283, Mar. 2010, doi: 10.1109/TCST.2010.2043926.

[68] Z. Zhang, Y. Niu, and J. Song, "Input-to-state stabilization of interval type-2 fuzzy systems subject to cyberattacks: An observer-based adaptive sliding mode approach," *IEEE Transactions on Fuzzy Systems*, vol. 28, no. 1, pp. 190–203, Jan. 2019, doi: 10.1109/TFUZZ.2019.2902845.

[69] Z. Song, J. Liu, Y. Liu, Y. Hu, and F. Fang, "Fault-tolerant control of floating wind turbine with switched adaptive sliding mode controller," *IEEE Transactions on Automation Science and Engineering*, vol. 21, no. 3, pp. 3705–3718, Jul. 2023, doi: 10.1109/TASE.2023.3332975.

[70] B. He and F. Gao, "Influence analysis of leader information with application to formation control of multi-agent systems," *International Journal of Control, Automation and Systems*, vol. 18, no. 12, pp. 3062–3072, Dec. 2020, doi: 10.1007/s12555-019-1037-x.

[71] M. Nazifi and M. Pourgholi, "Adaptive Fractional-Order Consensus Control of Cyber-Physical Power Systems in the Presence of Unbounded Perturbations," *International Journal of Industrial Electronics Control & Optimization*, vol. 8, no. 2, pp. 95–108, 2025, doi: 10.22111/ieco.2025.48713.1542.

[72] Q. Li, H. Wei, D. Hua, J. Wang, and J. Yang, "Stabilization of semi-Markovian jumping uncertain complex-valued networks with time-varying delay: A sliding-mode control approach," *Neural Processing Letters*, vol. 56, no. 2, p. 111, Apr. 2024, doi: 10.1007/s11063-024-11546-8.

[73] M. Roohi, S. Mirzajani, and A. Basse-O'Connor, "A no-chatter single-input finite-time PID sliding mode control technique for stabilization of a class of 4D chaotic fractional-order laser systems," *Mathematics*, vol. 11, no. 21, p. 4463, Oct. 2023, doi: 10.3390/math11214463.

[74] J. Gao, Z. Chu, L. Chen, M. Zhu, and B. Chen, "Cooperative control of multiple ball screws based on fractional-order composite controller," *Asian Journal of Control*, vol. 27, no. 1, pp. 658–670, Jan. 2025, doi: 10.1002/asjc.3440.

[75] A. Stephen, K. Rajakopal, R. Raja, A. Srinidhi, K. Thamilmaran, and R. P. Agarwal, "Non-fragile reliable control for multi-agent systems with actuator faults using an improved LK functional," *Nonlinear Dynamics*, vol. 113, no. 7, pp. 6645–6669, 2025, doi: 10.1007/s11071-025-10125-4.

[76] A. Liu, H. Yang, and L. Xiang, "Distributed Adaptive Fixed-Time Hierarchical Sliding Mode Control for High-Order Nonlinear Multi-

agent Systems," in *International Conference on Advanced Robotics, Control, and Artificial Intelligence*, pp. 1070–1081, 2024, doi: 10.1007/978-981-96-2058-1_96.

[77] R. Kavikumar, O. M. Kwon, S. H. Lee, and R. Sakthivel, "Input-output finite-time IT2 fuzzy dynamic sliding mode control for fractional-order nonlinear systems," *Nonlinear Dynamics*, vol. 108, no. 4, pp. 3745–3760, 2022, doi: 10.1007/s11071-022-07355-0.

[78] J. Xu, Y. Niu, and H. K. Lam, "Event-triggered sliding mode control of fuzzy systems via artificial time-delay estimation," *IEEE Transactions on Fuzzy Systems*, vol. 29, no. 9, pp. 2467–2478, Sep. 2020, doi: 10.1109/TFUZZ.2020.3010908.

[79] B. Huang, Y. Liu, L. Glielmo, and W. Gui, "Fixed-time distributed robust optimization for economic dispatch with event-triggered intermittent control," *Science China Technological Sciences*, vol. 66, no. 5, pp. 1385–1396, May 2023, doi: 10.1007/s11431-022-2335-8.

[80] A. Sinha and R. K. Mishra, "Consensus tracking in multi agent system with nonlinear and non identical dynamics via event driven sliding modes," *arXiv preprint arXiv:1712.01152*, Dec. 2017.

[81] A. Sharifi, A. Sharafian, and Q. Ai, "Observer-based control for consensus tracking of non-linear synchronous generators system using sliding mode method and a radial basis function neural network," *The European Physical Journal Special Topics*, vol. 234, no. 15, pp. 3951–3972, 2025, doi: 10.1140/epjs/s11734-025-01793-w.

[82] C. Aouiti, Q. Hui, H. Jallouli, and E. Moulay, "Sliding mode control-based fixed-time stabilization and synchronization of inertial neural networks with time-varying delays," *Neural Computing and Applications*, vol. 33, no. 18, pp. 11555–11572, Sep. 2021, doi: 10.1007/s00521-021-05880-4.

Source details

Journal of Robotics and Control (JRC)

Years currently covered by Scopus: from 2020 to 2025

Publisher: Department of Agribusiness, Universitas Muhammadiyah Yogyakarta

ISSN: 2715-5056 E-ISSN: 2715-5072

Subject area: Engineering: Control and Systems Engineering | Computer Science: Artificial Intelligence

Source type: Journal

View all documents > | Set document alert | Save to source list

CiteScore 2024
6.5

SJR 2024
0.435

SNIP 2024
1.130

CiteScore | CiteScore rank & trend | Scopus content coverage

CiteScore 2024

6.5 = 2,827 Citations 2021 - 2024 / 436 Documents 2021 - 2024

Calculated on 05 May, 2025

CiteScoreTracker 2025

6.6 = 3,282 Citations to date / 497 Documents to date

Last updated on 05 January, 2026 • Updated monthly

CiteScore rank 2024

Category	Rank	Percentile
Engineering Control and Systems Engineering	#85/375	77th
Computer Science Artificial Intelligence	#139/450	69th

View CiteScore methodology > CiteScore FAQ > Add CiteScore to your site